Research Article Vol. 14, No. 8 / 1 Aug 2023 / Biomedical Optics Express 3924
Biomedical Optics EXPRESS

Orbital angular momentum mode fiber force sensing technology based on intensity interrogation

SHUHAN LYU,[1,4] YAOJUN GUAN,[2,3,5] AND XINGHUA SHI[3,6]

[1]West Nottingham Academy, Colora MD,21917, USA
[2]College of Science, China Agricultural University, Beijing, 100083, China
[3]Laboratory of Theoretical and Computational Nanoscience, Chinese Academy of Sciences (CAS) Key Laboratory for Nanosystem and Hierarchy Fabrication, CAS Center for Excellence in Nanoscience, National Center for Nanoscience and Technology, Chinese Academy of Sciences, Beijing 100190, China
[4]slyu@wna.org
[5]s20223102195@cau.edu.cn
[6]shixh@nanoctr.cn

Abstract: Micromanipulation and biological, materials science, and medical applications often require controlling or measuring the forces exerted on small objects. Based on the high linearity and sensitivity of OAM beams in the sensing field, this article proposes for the first time to apply OAM beams to force sensing. In this paper, a fiber optic force sensing technology based on the intensity distribution change of orbital angular momentum (OAM) mode is proposed and realized. This technique detects the magnitude of the external force applied to the fiber by exciting the OAM mode with a topological charge 3, thereby tracking changes in light intensity caused by mode coupling. Applying this technique to force measurement, we have experimentally verified that when the sensor is subjected to a force in the range of 0mN to 10mN, the change in speckle light intensity at the sensor output has a good linear relationship with the force. Meanwhile, theoretical analysis and experimental results indicate that compared with previous force sensing methods, this sensing technology has a simple structure, is easy to implement, has good stability, and has practical application potential.

1. Introduction

With the current trend of miniaturization of devices, micro manipulation has attracted widespread attention in recent years. In the micro world, reliable detection and control of contact forces is necessary because contact forces are easily damaged objects [1]. In many fields, such as micro systems [2], hydraulic sample testing [3], hydraulic fluid systems [4], hydraulic assembly [5], medicine [6], and material science [7], high sensitivity micro force sensors are required. For example, in medical cardiac catheterization, it is important to understand the contact force between the catheter and the blood vessel wall, which helps to avoid damaging the patient's fine blood vessel network. Compared with other force sensors, fiber optic force sensors have advantages such as high sensitivity, strong flexibility, light weight, compact structure, good biocompatibility, and resistance to electromagnetic interference. In the past few years, various fiber optic force sensors have been reported. For example, M. Krehel et al. achieved a sensing sensitivity of 3/ N by changing the material of the optical fiber [8], X. Hu et al. achieved a sensing sensitivity of 2.54/ N by adding micro perforations to the fiber [9], and C. Y. Shen et al. achieved a sensing sensitivity of 0.1/ mN by using fiber Bragg gratings [10]. There are still many practical design reports on the structure of force fiber optic sensing, such as linear stepped graded index fibers [8], coiled [9], polarized birefringence [11], fiber Bragg gratings [12], Fabry Perot [13], and distributed Bragg reflectors [14]. These force sensors mostly use Gaussian beam. To improve its sensitivity, they have modified the fiber optic structure, so most of them have

#495034 https://doi.org/10.1364/BOE.495034
Journal © 2023 Received 8 May 2023; revised 29 May 2023; accepted 31 May 2023; published 6 Jul 2023

Biomedical Optics EXPRESS

complex structures and high costs. To ensure that the sensitivity of force sensors using ordinary straight fiber structures can reach the level of force sensors using complex fiber structures, OAM beams are introduced into force fiber sensing.

Orbital angular momentum (OAM) beam is a kind of beam with a spiral phase front end, which is generally used as $e^{il\varphi}$. Where l represents the topological charge number, φ is the azimuth angle. This special phase structure leads to phase singularities and a doughnut like intensity distribution of OAM beams. Because of its unique structure, OAM beam is widely used in optical tweezers [15], nonlinear optics [16], quantum information processing [17], optical data storage [18] and transmission [19] due to its unique optical field mode and wavefront characteristics, especially in optical sensing [20–22]. For example, OAM beams have been used to measure object rotation based on Doppler frequency shifts without requiring complex object image reconstruction, while OAM based technologies extend a new optical degree of freedom perspective to detect lateral motion in any direction. In addition, magnetic field measurements apply an OAM mode with opposite propagation directions, which interferes with the formation of petal shaped images. An optical fiber sensor based on OAM mode is proposed and implemented by tracking the rotation angle of the spiral interference pattern generated by coaxial interference between OAM mode and Gaussian beam, as well as tracking the intensity changes of the coherent superposition state between the fundamental mode and OAM mode with a topological load of 1, to sense the external parameters applied to the grating region.

OAM beams can be used in micro-force transducers as well. When an incoming beam is tilted or obstructed, its OAM spectrum, which is the optical power in each of OAM states, can vary due to extrinsic OAM properties that are associated with the variations in the beam's center of gravity, as well as the intrinsic OAM assets designated by the azimuthal phase factors. The phase-change rate of each OAM mode would be proportional to its order, which indicates that a higher-order OAM beam has a smaller phase-change spatial periodicity [23]. In addition, an OAM mode is moderately stable in any homogeneous medium, which specifies that the amount of OAM of a beam could be constant during propagation regardless of any beam diffraction [24]. Due to the different propagation constants of each mode in the fiber, changes in the external environment can cause coupling between adjacent modes, which will result in changes in the spatial distribution of the output light field. Therefore, based on the above advantages of OAM beam, changes in environmental parameters can be measured by directly detecting changes in the output speckle image. This method is cheaper and more responsive than previous spectral detection.

Since the spatiotemporal characteristics of the speckle field are influenced by the light-guided conditions, variations in the speckle map can be linked to the magnitude of the external stimulus applied to the fiber [25]. Demodulation applications for speckle in fiber optic sensors have been shown to assess the sensitivity of sensors to external physical variables, including micro-displacement [26], vibration [27], temperature [28]. Practical applications in human-computer interaction have also been reported, such as tactile arrays [29] and devices for assessing hand movements [30], among others. Here, we propose a newly developed OAM beam fiber optic force sensor that measures the changes in speckle under different forces to obtain its sensitivity. Compared with the previous Gaussian beam, the speckle generated by OAM beam is more stable and accurate, and easy to analyze.

This paper proposes a coupling effect between modes by tracking the modes of OAM beams with a topological charge of 3. The spiral phase plate of a single optical route consists of a 16 cm ring core fiber used to directly excite the OAM mode with a topological charge of 3. When there is no external force, the two modes of OAM with a topological charge of 3 will not interfere with each other. When there is an external force, the phenomenon of coupling between the two modes will occur. As the force increases, the number of coupling modes increases. Here, we measure the sensor's ability by its resolution and sensitivity. The resolution here refers to the ability of the meat sensor to detect the minimum change in input within the specified measurement range,

Biomedical Optics EXPRESS

while sensitivity refers to the ratio of the output change of the sensor to the input change under steady-state operating conditions. The application of sensing technology in force measurement shows that in the range of 0 mN to 10 mN, the sensitivity and resolution are 0.02 /mN and 1 mN, respectively. At the same time, the linear fitting results show that there is a linear relationship between the strength change and the force.

2. Theoretical analysis

An OAM beam exhibits annular light intensity and spiral phase. The intrinsic modes in the fiber are classified into three categories, namely TE mode, TM mode and mixed mode (EH mode or HE mode). In the process of fiber transmission, the TE and TM modes are linearly polarized waves whose polarization directions are orthogonal to each other. EH and HE modes are elliptically polarized waves. Equation (1) is the expression of an OAM beam formed by the combination of mixed modes in the optical fiber eigenmode in an optical fiber [31,32]. Here l is the angular modulus or time-topological charge, and n is the radial modulus.

$$\begin{cases} OAM_{l,n} = HE^{even}_{l+1,n} \pm iHE^{odd}_{l+1,n} \\ OAM_{l,n} = EH^{even}_{l-1,n} \pm iEH^{odd}_{l-1,n} \end{cases} \tag{1}$$

Specifically, The OAM mode is formed by superposition of homogeneous intrinsic odd-even modes with phase difference $\pi/2$. The odd and even modes are the components of the electromagnetic field in two perpendicular directions. In Eq. (1), HE^{even} and HE^{odd} (EH^{even} and EH^{odd}) represents the even mode and odd mode of HE mode (or EH mode), respectively, and indicate the topological charge of the OAM beam. This expression describes the transmission state of OAM beam when the topological charge is greater than 1 in the fiber. In optical fibers, the transmission constant difference between adjacent mode pairs is small, such as modes HE_{41} and EH_{21} covered in this article, and mode coupling is more likely to occur when external perturbations are applied due to the smaller transmission constant between adjacent mode pairs [33]. When two modes are coupled, their mode will change to LP mode, as follows

$$\begin{cases} LP_{3,1} = HE^{even}_{4,1} \pm iEH^{even}_{2,1} \\ LP_{3,1} = HE^{odd}_{4,1} \pm iEH^{odd}_{2,1} \end{cases} \tag{2}$$

The transmission constant is an important parameter for judging the coupling of the two modes, and here we can obtain the conduction constant of the corresponding mode by deriving the characteristic equations satisfied by the EH mode and the HE mode and solving them.

The derivation procedures of characteristic equation include the derivation of Helmholtz equations and the concrete forms of the longitudinal components E_z and H_z of the electromagnetic field. Then, the concrete form of E_z and H_z are substituted into Maxwell's equation to obtain the transverse components E_r, E_e, H_r, H_e. Finally, the mode characteristic equation is obtained by using the electromagnetic field H_θ and tangential continuous conditions on the interface.

Based on Maxwell's equation, Helmholtz equation and boundary conditions, scalar Helmholtz equation in cylindrical coordinate system can be obtained

$$\nabla^2\psi - \frac{n^2}{c^2}\frac{\partial^2\psi}{\partial t^2} = 0 \tag{3}$$

where ψ represents the field component, c is the speed of light in a vacuum, and n is the refractive index.

Biomedical Optics EXPRESS

Using Bessel function to express the field in an annular fiber, we have(4)

$$\begin{cases} \psi_1 = C_1 I_m(wr)\, exp(im\varphi) exp\{-i(\omega t - \beta z)\} & r<r_2 \\ \psi_2 = \{C_2 J_m(ur) + C_3 Y_m(ur)\}\, exp(im\varphi) exp\{-i(\omega t - \beta z)\} & r_2<r<r_1 \\ \psi_3 = C_4 K_m(wr)\, exp(im\varphi) exp\{-i(\omega t - \beta z)\} & r_1<r \end{cases} \tag{4}$$

The normalized radial phase constant u and the normalized attenuation constant w of the guided wave satisfy

$$\begin{cases} u^2 = (n_2^2 k^2 - \beta^2) \cdot \frac{v^2}{n_1^2 - n_2^2} \\ w^2 = (\beta^2 - n_1^2 k^2) \cdot \frac{v^2}{n_1^2 - n_2^2} \end{cases} \tag{5}$$

v is the normalized frequency, $C_1, C_2,\ C_3$ *and* C_4 are arbitrary constants. Y is the second type of Bezier function, I is the first type of virtual Bezier function, r_2 is the inner diameter of the ring core and r_1 is the outer diameter of the ring core. Based on continuous boundary conditions, Eqs. (2)–(4), the considered constant can be written as

$$\begin{cases} C_2 = \frac{wI'_m(wr_1)Y_m(ur_1) - uI_m(wr_1)Y'_m(ur_1)}{uI_m(wr_1)J'_m(ur_1) - wI_m(wr_1)J_m(ur_1)} \\ C_1 = \frac{C_2 J_m(ur_1) + C_3 Y_m(ur_1)}{I_m(wr_1)} \\ C_4 = \frac{C_2 J_m(ur_2) + C_3 Y_m(ur_2)}{K_m(wr_2)} \end{cases} \tag{6}$$

To solve the above equations, write Eq. (5) in a matrix form and solve for zero determinant of the matrix, in this case, we arrive at the following characteristic equation

$$\begin{aligned} &[wI_m(wr_1)J_m(ur_1) - uI_m(wr_1)J'_m(ur_1)] \cdot [wK_m(wr_2)Y_m(ur_2) - uK_m(wr_2)Y'_m(ur_1)] - \\ &[wI_m(wr_1)Y_m(ur_1) - uI_m(wr_1)Y_m(ur_1)] \cdot [wK_m(wr_2)J_m(ur_2) - uK_m(wr_2)J'_m(ur_1)] = 0 \end{aligned} \tag{7}$$

The partial derivatives of Bessel function in the characteristic equation read

$$\begin{cases} J'_v(x) = \frac{1}{2}[J_{v-1}(x) - J_{v+1}(x)] \\ I'_v(x) = \frac{1}{2}[I_{v-1}(x) + I_{v+1}(x)] \\ Y'_v(x) = \frac{1}{2}[Y_{v-1}(x) - Y_{v+1}(x)] \\ K'_v(x) = -\frac{1}{2}[K_{v-1}(x) - K_{v+1}(x)] \end{cases} \tag{8}$$

From Eq. (6) we can easily get the transfer constants corresponding to the corresponding mode. Here, HE_{41} takes 4 for m, and EH_{21} takes 2 for m. We calculate the transmission constants of the two respectively to provide parameters for the design of the subsequent micro-bending deformer.

The application history of fiber optic micro bending sensors as a strength modulated fiber optic sensor can be traced back to the research on fiber optic sensor systems conducted by the US Naval Research Institute in 1977. When the micro-bending sensor is perturbed, the amount of bending of the sensitive optical fiber changes, and the optical fiber generates inter-mode coupling, and part of the energy is coupled from the core mode to the cladding mode, resulting in the core transmission energy loss. By establishing the relationship between external disturbance and optical power loss, the optical fiber micro bending sensor measures the change of output optical power at the optical detector end, to calculate the size of the external disturbance [34]. As shown in Fig. 1, the deformer used here is composed of a pair of toothed plates with a mechanical period of Λ, and the sensitive optical fiber passes through the middle of the toothed shape, resulting in

Biomedical Optics EXPRESS

periodic bending under the action of the toothed plate. When the toothed plate is subjected to external force, the degree of micro bending of the optical fiber changes, resulting in the change of output optical power, and the magnitude of the external force is indirectly measured by measuring the change of output optical power, to realize the function of micro-bending sensor.

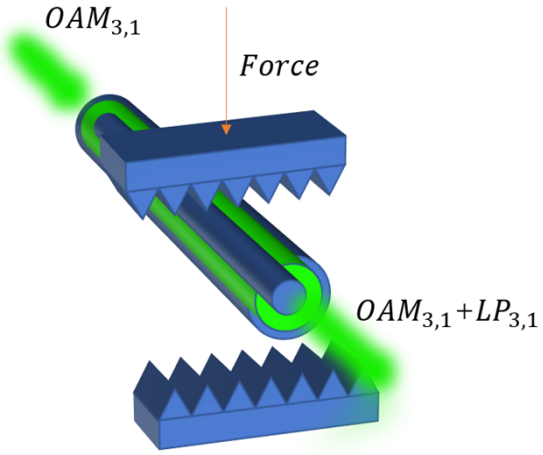

Fig. 1. Micro-bending deformer structure.

For two adjacent modes the propagation constant difference $\Delta\beta$ is given by

$$\delta\beta_c = \beta_{c+1} - \beta_c \tag{9}$$

where c is the ordinal of the modulus.

The realization of force micro bending allows the internal mode to be quickly coupled to achieve the resonant condition of the loss peak, and the pitch period needs to meet the following conditions

$$\delta\beta_c = 2\pi/\Lambda_c \tag{10}$$

The change in light transmission intensity through the micro bend sensor ΔI can be written [35]

$$\Delta I = \left(\frac{\Delta I}{\Delta X}\right) \Delta F(k_f + \frac{A_s Y_s}{l_s})^{-1} \tag{11}$$

where k_f is the mechanical constant of the curved fiber, As is the cross-sectional area of the fiber, Y_s is the Young's modulus of the fiber, and l_s is the length of the deformer. ΔF is the change in force, the deformation of the fiber becomes X, and its corresponding change is ΔX.

k_f is the effective spring constant of the fiber sandwiched between the deformers

$$k_f^{-1} = \frac{\Lambda_c^3}{3\pi Y d^4 \eta} \tag{12}$$

where Y is Young's modulus, d is the fiber diameter and η is the number of bends.

Among the above types $\Delta T/\Delta X$ is the sensitivity coefficient, and its value is closely related to the mechanical period Λ_c of the deformer. The sensor makes mode superposition coupling through external force, and the energy exchange generated during mode coupling leads to light energy loss. This loss is reflected in the variation of output light intensity. From Eq. (10), the change in external forces is directly proportional to the change in light intensity. Based on the OAM beam, when the OAM beam is subjected to external forces, the speckle caused by mode

Biomedical Optics EXPRESS

coupling becomes more stable and accurate, which has a more accurate and beneficial effect on subsequent speckle analysis. Here, we quantify the change in light intensity by changing the correlation coefficient to construct the relationship between light intensity and force. This is the principle of the force fiber optic sensor designed in this article. To further verify its feasibility, relevant experimental analysis was conducted next.

3. Details of the fiber optic force sensor microforce experiment

3.1. Construction and working principle

Fiber force sensing is divided into two processes: the first process is the modulation process of light waves by external forces, that is, external forces can change the transmission constant of the mode of optical fiber waves, causing adjacent modes to couple and thereby changing the output light intensity; The second process is the demodulation process, that is, detecting the modulated light wave signal and extracting the mechanical information acting on the sensor.

The most used optical fiber micro-force bending sensor principal diagram is shown in Fig. 1, the micro-bending structure in the figure is composed of a pair of toothed plates, the optical fiber passes through the middle of the toothed plate, and when a force is applied on the upper toothed plate, the optical fiber will be squeezed to produce periodic bending. In the test, a micro-force platform is applied to the moving toothed plate to generate a change in force. In order to ensure the accuracy of the experimental data, the toothed plate is selected with high-strength and low-elasticity materials, and when conditions permit, the optical fiber is pasted on the high-strength, low-elastic optical fiber reinforcement material, and the bending degree of the optical fiber is adjusted through the optical fiber reinforcement material, thereby changing its response sensitivity to external stress, and at the same time can effectively protect the optical fiber and extend its service life.

The experimental system device is shown in the figure, the laser emits a 1550 nm laser through the focusing lens coupled into the optical fiber, and then the optical fiber passes through the micro-force bending deformer, and the laser spot at the output end of the optical fiber is received with CCD, and finally the spot image is transmitted to the PC for observation, acquisition and storage. Figure 2 is schematic diagrams of OAM force fiber optic sensors, respectively. The sensing fiber of the OAM beam is a ring core fiber, and the fiber length is 16 cm. The ring core has a refractive index of 1.7, the cladding has a refractive index of 1.444, and the material is silica. The inner diameter is 3.5 microns, and the outer diameter is 5 microns. The topological charge of the OAM beam is 3 and the pitch is 1 mm.

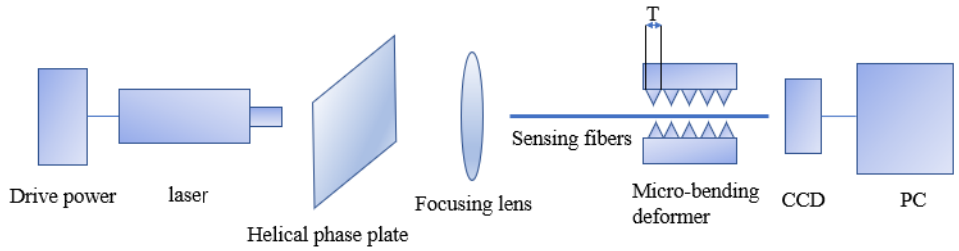

Fig. 2. OAM beam experimental setup.

3.2. Speckle analysis

By introducing an OAM beam into the ring core optical fiber for force sensing test, the response effect of the sensor is obtained by analyzing the change of the correlation coefficient of the

Biomedical Optics EXPRESS

speckle map obtained during the time-varying force, and the sensitivity of the sensor is obtained by fitting the change curve of force and correlation coefficient.

Our use of emerging speckle analysis sensing technology has many advantages for traditional sensors, they do not need to rely on expensive spectrometers for analysis, only need to use a lightweight camera, low cost, easy to carry, etc. The Pearson coefficient C is directly applied for correlation analysis and characterization, which simplifies the technical means of decoupling sensing information and shows very reliable advantageous results.

In terms of mathematical econometric relationships, the correlation function C is a common statistical ruler used to measure the correlation and independence of a series of variables, and explains the statistical relationship between multiple sets of values. The normalized covariance correlation function we use, also known as the "Pearson coefficient", can be used to measure the linear relationship between two sets of variables [36]. When two images have exactly the same features, the correlation function value between them is 1. If the two images are completely inconsistent, the correlation function value is 0. Therefore, when the external environmental conditions change, the speckle will also change, and the correlation function value between the target speckle and the reference speckle will be less than 1 and become smaller with the increase of the difference. Through such a relationship, we can quantitatively measure the changing factors of the sensing scene.

To further reduce the error and improve the accuracy, in our experiments, for each changing environmental condition, 10 speckle maps are sampled simultaneously at a certain frequency for averaging. For each sampled target speckle, the correlation coefficient is calculated one by one by the target speckle and each reference speckle map and then averaged to obtain more accurate results. For 10 target images acquired at time t under the condition, the value of the correlation coefficient under this condition is averaged by averaging the 100 correlation coefficients ΔC calculated one by one with 10 reference speckles. Through such sampling and calculation methods, the systematic error caused by data fluctuation can be appropriately reduced.

In the speckle correlation analysis method, the predefined correlation function is a function that evaluates the degree of match between the reference image and the sample image. Different correlation functions may correspond to different calculation accuracy and convergence speed, which will affect the calculation speed and accuracy of the sensor response to a certain extent. At present, there are more than ten forms of correlation functions mentioned in the literature. Generally, it is more common to normalize the covariance correlation function [28]

$$C = \frac{\sum_{k=1}^{N}\sum_{l=1}^{M}[I_R(k,l,t_0) - \bar{I}_R(t_0)][I_0(k,l,t) - \bar{I}_0(t)]}{\sqrt{\{\sum_{k=1}^{N}\sum_{l=1}^{M}[I_R(k,l,t_0) - \bar{I}_R(t_0)]^2\} * \{\sum_{k=1}^{N}\sum_{l=1}^{M}[I_0(k,l,t) - \bar{I}_0(t)]^2\}}} \tag{13}$$

where $I_R(k,l,t_0)$ and $I(k,l,t)$ are the light intensity of the reference speckle and the target speckle collected at the pixel (k,l) at the t_0 and t moments, respectively, (t_0 is the initial moment, t is the target speckle sampling time after the condition changes). $\bar{I}_R(t_0)$ and $\bar{I}(t)$ are the light intensity averages of the speckle map, respectively.

Here, to quantify the change in light intensity caused by force, the amount of change in the correlation coefficient is equivalent to the change in light intensity.

$$\Delta I = \Delta C = 1 - C \tag{14}$$

When multiple optical modes are transmitted in the fiber, the transmission conditions of the modes are changed due to the influence of the environment, resulting in crosstalk conversion and composition changes before the modes are compared to each other. Different modes of light field distribution are different, and the spot morphology is also different. The process of mode conversion also makes the change of light field strength manifest as the change of output speckle.

It is represented by the light intensity value recorded by each pixel. The idea of the design here is to use the change of laser speckle to analyze the above degree of change through correlation

Biomedical Optics EXPRESS

technology. According to the expression of Eq. (13), by comparing the speckle pattern recorded at different times with the initial recorded pattern, we can obtain the correlation coefficient C, and by analyzing the change law of C, we can reverse the state of the environmental variables at that time.

3.3. Experiment details

To characterize the relationship between force and the amount of change in correlation coefficient, here we obtain the sensitivity of this fiber optic sensor by linearly fitting between the force and its correlation coefficient.

Here, data is collected every 2 mN between 0 mN and 10 mN. The obtained set of speckle results is shown in Fig. 3.

Here, the experimental speckle map is converted into matrix form by MATLAB, and the correlation coefficient is calculated according to the Eq. (13), By comparing the speckle patterns recorded at different times with the initial recorded patterns, we can obtain the correlation coefficient C, and by analyzing the change law of C, we can deduce the state of the environmental variables at that time. To further reduce the error and improve the accuracy, in our experiments, for each changing environmental condition, 10 speckle maps are sampled simultaneously at a certain frequency for averaging. For each sampled target speckle, the correlation coefficient is calculated one by one by the target speckle and each reference speckle map and then averaged to obtain more accurate results. For 10 target images acquired at time t under the condition, the value of the correlation coefficient under this condition is averaged by averaging the 100 correlation coefficients ΔC calculated one by one with 10 reference speckles. Through such sampling and calculation methods, the systematic error caused by data fluctuation can be appropriately reduced.

Here we calculate the change ΔC of the above correlation coefficient and perform linear fitting on it. The fitting curve is shown in Fig. 4.

We calculated the correlation coefficient for speckle C, corresponding to the correlation coefficient of 0 to 10 mN. To quantify the force information, it is characterized by calculating the change in the correlation coefficient, ΔC. Then, the sensitivity of the sensor can be obtained by fitting the curve of the relevant point to calculate the slope. The curve in Fig. 4 characterizes the approximate linear positive correlation between the force change and the correlation coefficient change in the ring core fiber, the red line is the data fitting curve for OAM beam sensing, the sensitivity is about 0.02 /mN.

Here, to verify the stability and effectiveness of our designed sensor in practical applications, we conducted the following sensing experiments on the sensor to obtain the sensing effect of the sensor designed in this article on the sensor's changing force and time resolution. The OAM beam with a topological charge of 3 enters the ring core fiber for sensing, and the applied force exhibits a sine time function between 0 mN and 10 mN.

We apply a time-varying force of $F = 10|sin(\pi t/18)|$, record a speckle map from 0 to 18 seconds in CCD, apply a time-varying force of $F = 10|sin(\pi t/12)|$, record a speckle map from 0 to 12 seconds in CCD and apply a time-varying force of $F = 10|sin(\pi t/8)|$, record a speckle map from 0 to 8 seconds in CCD. We collect images once a second and input them into MATLAB to obtain their grayscale matrix. Compare each image with the initial image, calculate its correlation coefficient, and obtain the change in correlation coefficient. Then we analyze the linear change of speckle light intensity of this sensor under the action of sinusoidal force. The result graph is shown as

We tested the force sensing element with loads of different frequencies. As an example, the force response of sensors at three different frequencies is presented, and the graphs show the process of compression loading and unloading of the optical fiber. The solid line in Fig. 5 represents the load curve of a sinusoidal force of $F = 10|sin(\pi t/8)|$, the dashed line represents the load curve of a sinusoidal force of $F = 10|sin(\pi t/12)|$, and the dotted line represents the

Biomedical Optics EXPRESS

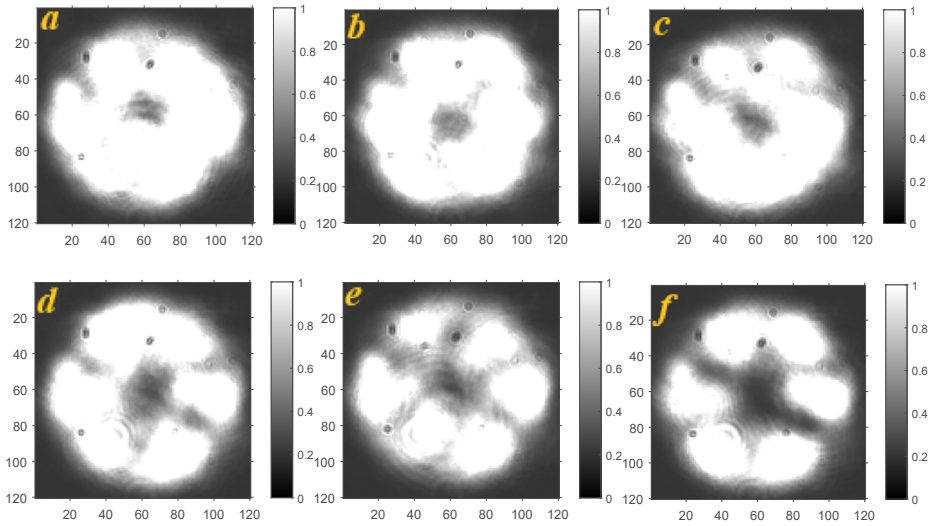

Fig. 3. Experimental results of OAM force sensing speckle. (a) is the speckle scattering obtained when the fiber is subjected to a force of 0 mN. (b) is the speckle scattering obtained when the fiber is subjected to a force of 2 mN. (c) is the speckle scattering obtained when the fiber is subjected to a force of 4 mN. (d) is the speckle scattering obtained when the fiber is subjected to a force of 6 mN. (e) is the speckle scattering obtained when the fiber is subjected to a force of 8 mN. (f) is the speckle scattering obtained when the fiber is subjected to a force of 10 mN).

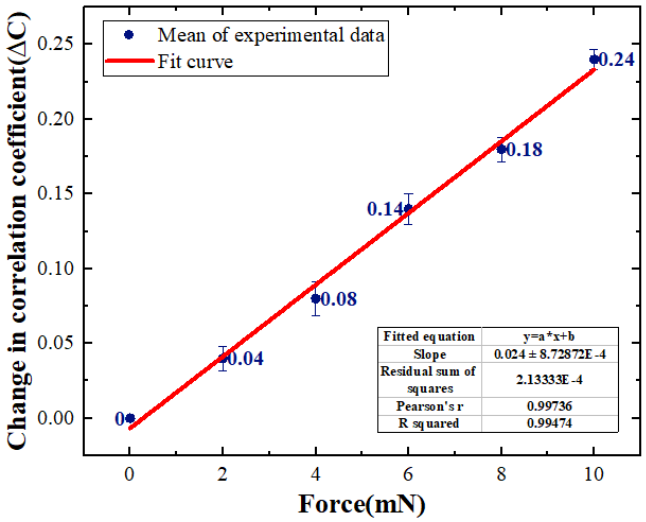

Fig. 4. The fitting curve of the mean of the correlation coefficient change and the error bar of the experimental data.

load curve of a sinusoidal force of $F = 10|sin(\pi t/18)|$. In Fig. 5, the pentagram point is the data point calculated under the action of sine force $F = 10|sin(\pi t/8)|$, the circular point is the data point calculated under the action of sine force $F = 10|sin(\pi t/12)|$, and the quadrilateral point is the data point calculated under the action of sine force $F = 10|sin(\pi t/18)|$. There is a good correlation between the variation value of the calculated correlation coefficient (represented by

Biomedical Optics EXPRESS

dots) and the applied force (line). Under the compression and decompression training of optical fibers, the calculated correlation coefficient changes exhibit a linear response within the test load range without significant lag, thus providing reliable force readings that are crucial for sensor performance. Please note that in all force measurements discussed here, the temperature of the surrounding environment of the sensor is kept constant to avoid the additional impact of temperature on resonant displacement.

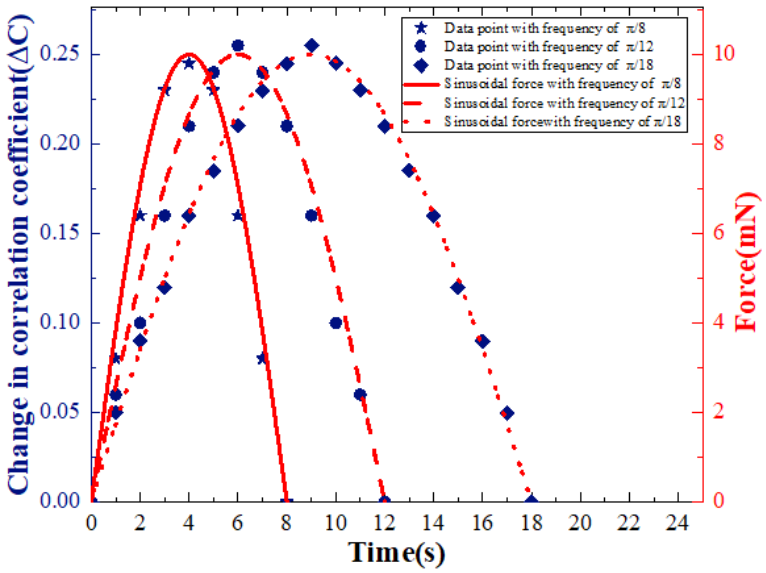

Fig. 5. The response of the sensor under the action of sinusoidal force load. The solid line represents the load curve of a sinusoidal force of $F = 10|sin(\pi t/8)|$, the dashed line represents the load curve of a sinusoidal force of $F = 10|sin(\pi t/12)|$, and the dotted line represents the load curve of a sinusoidal force of $F = 10|sin(\pi t/18)|$. the pentagram point is the data point calculated under the action of sine force $F = 10|sin(\pi t/8)|$, the circular point is the data point calculated under the action of sine force $F = 10|sin(\pi t/12)|$, and the quadrilateral point is the data point calculated under the action of sine force $F = 10|sin(\pi t/18)|$.The coincidence of the two indicates that there is a good linear relationship between the force and the light intensity, and the degree of response to the force is high.

4. Conclusion

In this paper, a fiber optic force sensing concept based on OAM beam is proposed, which is characterized by measuring the micro-force bending of the ring-core fiber entering the OAM beam with a micro bending deformer. In the fiber with a length of 16 cm, the fibers present different spot patterns by slight force bending, because the spot pattern presented by OAM in external perturbations is very stable, so the magnitude of the force can be characterized by direct analysis of the light intensity change of the speckle map, which is a simpler and more efficient demodulation method. After analyzing the speckle map, the minimum change in input quantity that the sensor can detect is 10^{-3}N, and the sensitivity reaches 0.02 /mN after analyzing the speckle map. Compared with other complex structures to achieve high sensitivity force sensors, the OAM fiber optic force sensor proposed in this paper only changes the beam type but achieves the same or even higher sensitivity as other force sensors with complex structure, which has certain reference significance for the subsequent research of high sensitivity force sensors.

Biomedical Optics EXPRESS

Acknowledgments. Thank Professor Feng Xiqiao of Tsinghua University for his guidance.

Disclosures. The authors declare no conflicts of interest.

Data availability. Data underlying the results presented in this paper are not publicly available at this time but may be obtained from the authors upon reasonable request.

References

1. Y. Z. Wei and Q. S. Xu, "An overview of micro-force sensing techniques," Sens. Actuators, A **234**, 359–374 (2015).
2. H. Conrad, H. Schenk, B. Kaiser, S. Langa, M. Gaudet, K. Schimmanz, and M. Lenz, "A small-gap electrostatic micro-actuator for large deflections," Nat. Commun. **6**(1), 10078 (2015).
3. Y. Xie, Y. Zhou, Y. Lin, L. Wang, and W. Xi, "Development of a microforce sensor and its array platform for robotic cell microinjection force measurement," Sensors **16**(4), 483 (2016).
4. K. Uhrig, R. Kurre, C. Schmitz, J. E. Curtis, T. Haraszti, A. E. M. Clemen, and J. P. Spatz, "Optical force sensor array in a microfluidic device based on holographic optical tweezers," Lab Chip **9**(5), 661–668 (2009).
5. Z. Hu, W. Fang, Q. Li, X. Q. Feng, and J. A. Lv, "Optocapillarity-driven assembly and reconfiguration of liquid crystal polymer actuators," Nat. Commun. **11**(1), 5780 (2020).
6. H. Guo, Y. J. Tan, G. Chen, Z. Wang, G. J. Susanto, H. H. See, Z. Yang, Z. W. Lim, L. Yang, and B. C. Tee, "Artificially innervated self-healing foams as synthetic piezo-impedance sensor skins," Nat. Commun. **11**(1), 5747 (2020).
7. Q. Zhu, K. Van Vliet, N. Holten-Andersen, and A. Miserez, "A double-layer mechanochromic hydrogel with multidirectional force sensing and encryption capability," Adv. Funct. Mater. **29**(14), 1808191 (2019).
8. M. Krehel, R. M. Rossi, G.-L. Bona, and L.J. Scherer, "Characterization of flexible copolymer optical fibers for force sensing applications," Sensors **13**(9), 11956–11968 (2013).
9. X. Hu, D. Saez-Rodriguez, C. Marques, O. Bang, D. Webb, P. Mégret, and C. Caucheteur, "Polarization effects in polymer FBGs: study and use for transverse force sensing," Opt. Express **23**(4), 4581–4590 (2015).
10. X. Gui, M. Galle, L. Qian, W. Liang, C. Zhou, Y. Ou, and D. Fan, "Demodulation method combining virtual reference interferometry and minimum mean square error for fiber-optic Fabry–Perot sensors," Chin. Opt. Lett. **16**, 010606 (2018).
11. Y. Gong, C. Yu, T. Wang, X. Liu, Y. Wu, Y. Rao, M. Zhang, H. Wu, X. Chen, and G. Peng, "Highly sensitive force sensor based on optical microfiber asymmetrical Fabry–Pérot interferometer," Opt. Express **22**(3), 3578–3584 (2014).
12. J. C. Vieira, O. M. F. Morais, C. M. A. Vasques, and R. de Oliveira, "A laboratorial prototype of a weight measuring system using optical fiber Bragg grating sensors embedded in silicone rubber," Measurement **61**, 58–66 (2015).
13. S. Pirozzi, "Multi-point force sensor based on crossed optical fibers," Sens. Actuators, A **183**, 1–10 (2012).
14. K. Yu, C. Wu, M. Sun, C. Lu, H. Tam, Y. Zhao, and L. Shao, "Fiber laser sensor for simultaneously axial strain and transverse load detection," Measurement **62**, 137–141 (2015).
15. M. Padgett and R. Bowman, "Tweezers with a twist," Nat. Photonics **5**(6), 343–348 (2011).
16. D. Ding, Z. Zhou, B. Shi, X. Zou, and G. Guo, "Linear up-conversion of orbital angular momentum," Opt. Lett. **37**(15), 3270–3272 (2012).
17. Z. Y. Zhou, Y. Li, D. S. Ding, W. Zhang, S. Shi, and B. S. Shi, "Orbital angular momentum photonic quantum interface," Light: Sci. Appl. **5**(1), e16019 (2016).
18. G. Gibson, J. Courtial, M. Padgett, M. Vasnetsov, V. Pas'ko, S. Barnett, and S. Franke-Arnold, "Free-space information transfer using light beams carrying orbital angular momentum," Opt. Express **12**(22), 5448–5456 (2004).
19. H. Huang, G. Xie, Y. Yan, N. Ahmed, Y. Ren, Y. Yue, D. Rogawski, M. Willner, B. Erkmen, K. Birnbaum, S. Dolinar, M. Lavery, M. Padgett, M. Tur, and A. Willner, "100 Tbit/s free-space data link enabled by three-dimensional multiplexing of orbital angular momentum, polarization, and wavelength," Opt. Lett. **39**(2), 197–200 (2014).
20. L. Wang, W. Zhang, B. Wang, L. Chen, Z. Bai, S. Gao, J. Li, Y. Liu, L. Zhang, Q. Zhou, and T. Yan, "Simultaneous strain and temperature measurement by cascading few-mode fiber and single-mode fiber long-period fiber gratings," Appl. Opt. **53**(30), 7045–7049 (2014).
21. J. Zhao, J. Xu, C. Wang, Y. Liu, and Z. Yang, "Experimental demonstration of multi-parameter sensing based on polarized interference of polarization-maintaining few-mode fibers," Opt. Express **28**(14), 20372–20378 (2020).
22. Q. Ling and Z. Gu, "Simultaneous detection of SRI and temperature with a FM-LPFG sensor based on dual-peak resonance," J. Opt. Soc. Am. B **36**(8), 2210–2215 (2019).
23. Z. S. Eznaveh, J. C. A. Zacarias, J. E. A. Lopez, K. Shi, G. Milione, Y. Jung, B. C. Thomsen, D. J. Richardson, N. Fontaine, S. G. Leon-Saval, and R. Amezcua Correa, "Photonic lantern broadband orbital angular momentum mode multiplexer," Opt. Express **26**(23), 30042–30051 (2018).
24. Y. Shen, X. Wang, Z. Xie, C. Min, X. Fu, Q. Liu, M. Gong, and X. Yuan, "Optical vortices 30 years on: OAM manipulation from topological charge to multiple singularities," Light: Sci. Appl. **8**(1), 90 (2019).
25. A. Souto Janeiro, A. Fernández López, M. Chimeno Manguan, and P. Pérez-Merino, "Three-dimensional digital image correlation based on speckle pattern projection for non-invasive vibrational analysis," Sensors **22**(24), 9766 (2022).
26. M. J. Murray, A. Davis, C. Kirkendall, and B. Redding, "Speckle-based strain sensing in multimode fiber," Opt. Express **27**(20), 28494–28506 (2019).

Biomedical Optics EXPRESS

27. E. Fujiwara, Y. T. Wu, and C. K. Suzuki, "Vibration-based specklegram fiber sensor for measurement of properties of liquids," Opt. Lasers Eng. **50**(12), 1726–1730 (2012).
28. J. J. Wang, S. C. Yan, Y. P. Ruan, F. Xu, and Y. Q. Lu, "Fiber-optic point-based sensor using specklegram measurement," Sensors **17**(10), 2429 (2017).
29. F. Feng, W. Chen, D. Chen, W. Lin, and S. C. Chen, "In-situ ultrasensitive label-free DNA hybridization detection using optical fiber specklegram," Sens. Actuators, B **272**, 160–165 (2018).
30. Z. Ding and Z. Zhang, "2D tactile sensor based on multimode interference and deep learning," Opt. Laser Technol. **136**, 106760 (2021).
31. C. Brunet and L. A. Rusch, "Optical fibers for the transmission of orbital angular momentum modes," Opt. Fiber Technol. **35**, 2–7 (2017).
32. C. Brunet, P. Vaity, Y. Messaddeq, S. LaRochelle, and L. A. Rusch, "Design, fabrication and validation of an OAM fiber supporting 36 states," Opt. Express **22**(21), 26117–26127 (2014).
33. M. Wei, G. Tang, J. Liu, L. Zhu, J. Liu, C. Huang, J. Zhang, L. Shen, and S. Yu, "Neural network-based perturbation-location fiber specklegram sensing system towards applications with limited number of training samples," J. Lightwave Technol. **39**(19), 6315–6326 (2021).
34. Y. Yuan, G. Wu, X. Li, Y. Fan, and X. Wu, "Effects of twisting and bending on LP 21 mode propagation in optical fiber," Opt. Lett. **36**(21), 4248–4250 (2011).
35. J. W. Berthold, "Historical review of microbend fiber-optic sensors," J. Lightwave Technol. **13**(7), 1193–1199 (1995).
36. E. Fujiwara, Y. Ri, Y. T. Wu, H. Fujimoto, and C. K. Suzuki, "Evaluation of image matching techniques for optical fiber specklegram sensor analysis," Appl. Opt. **57**(33), 9845–9854 (2018).